crystals

MDPI

Article

Potentials and Limits of PMN-PT and PIN-PMN-PT Single Crystals for Pyroelectric Energy Harvesting

Mohammed Es-Souni

Institute for Materials & Surface Technology, Honorary Member of Kiel University of Applied Sciences, 24149 Kiel, Germany; mohammed.es-souni@fh-kiel.de

Abstract: Waste heat is inherent to industrial activities, IT services (e.g., data centers and microprocessors), human mobility, and many other common processes. The power lost each year in this way has been estimated in the 1000 TWh in the EU which, owing to skyrocketing energy prices and not least the urgent need for decarbonizing the economy, has engendered tremendous research efforts among scientists and engineers to recover/recycle this waste energy. Beyond established thermal engineering solutions for waste heat, advances in multifunctional materials open new paradigms for waste heat harvesting. Two smart material types are of particular focus and interest at present; these are thermoelectric and pyroelectric materials, which can both transform heat to electrical power, though via different effects. The present paper summarizes our research work on a new class of pyroelectric materials, namely <111> oriented $(1-x)(Pb(Mg_{1/3}Nb_{2/3})O_3–xPbTiO_3$ (PMN-PT) and x-$Pb(In_{1/2}\ Nb_{1/2})O_3$-y-$Pb(Mg_{1/3}\ Nb_{2/3})O_3$-(1 − x − y)-$PbTiO_3$ (PIN-PMN-PT) single crystals that exhibit some of the highest pyroelectric properties ever measured. First, a figure of merit for pyroelectric energy harvesting is derived, followed by a detailed assessment of the properties of the said crystals and how they depend on structure, poling, thickness, and temperature. The properties are further contrasted with those of conventional pyroelectric crystals. It is concluded that the PMN-PT-base single crystals are best suited for harvesting devices with a working temperature range from 40 to 100 °C, which encompasses waste heat generated by data centers and some chemical and industrial processes, affording the highest figure of merit among pyroelectric materials.

Keywords: PMN-PT-base single crystals; pyroelectric energy harvesting; figure of merit; ferroelectrics; polarization; pyroelectric coefficient

Citation: Es-Souni, M. Potentials and Limits of PMN-PT and PIN-PMN-PT Single Crystals for Pyroelectric Energy Harvesting. *Crystals* **2024**, *14*, 236. https://doi.org/10.3390/cryst14030236

Academic Editor: Zhonghua Yao

Received: 27 December 2023
Revised: 22 February 2024
Accepted: 25 February 2024
Published: 28 February 2024

1. Introduction

Waste energy is ubiquitous in industrial and human processes. Waste thermal and mechanical energies are prominent among them, and research into means of converting them to electricity to power devices or recovering them for heating or cooling of buildings have been constantly growing over the last few decades [1,2]. The impetus for further research in this area comes from the simple need to improve energy management, reduce burnable fuels in the energy mix, and lastly to achieve progress towards decarbonizing the economy.

With respect to conversion of waste heat and mechanical vibrations to useful energy, multifunctional materials, whether they be ceramics, polymers, or nanocomposites, are playing a pivotal role. Thermoelectric and pyroelectric materials can convert waste heat to power via the Seebeck [3] and pyroelectric effect [4], respectively, without the necessity for moving parts, and thus are simple, lasting, maintenance-free, and afford the possibility for miniaturization to self-power small, microscopic, and embedded devices [3,5]. Stray mechanical vibrations from all sorts of human, industrial, and transport activities can be converted to electrical power using piezoelectric energy harvesters that have been known of and examined since the 1960s. Research around these harvesters has recently undergone a recrudescence of interest [6].

The suitability of a multifunctional material for a mode of energy harvesting depends on its coupled functional properties to generate maximum energy output; this can be summarized in figures of merit (FOM), which consider solely the materials' properties that are involved in the expression of energy output.

In the following, emphasis is placed on pyroelectric materials, especially PMN-PT base single crystals. Various aspects of the application of these crystals to energy harvesting devices are integrated in this paper, among them the structure-properties interrelationship, property control via poling and ageing, and thickness effects. The results reported here were garnered in the last few years, as part of the framework of various projects funded by the German federal government.

Figure of Merit (FOM) for Pyroelectric Energy Harvesting

Pyroelectric materials are polar materials that convert incident heat waves/infrared radiation to electrical power/signals through the temperature dependence of their spontaneous polarization, P_s. The total electric displacement D is given by Equation (1), where E is the electric field and ε the permittivity [4]:

$$D = \epsilon E + P_s \tag{1}$$

As the temperature variation of D at constant stress and constant E is given by

$$\frac{\partial D}{\partial T} = \frac{\partial P_s}{\partial T} + E\frac{\partial \varepsilon}{\partial T} \tag{2}$$

a generalized pyroelectric coefficient p_g can be defined as:

$$p_g = p + E\frac{\partial \varepsilon}{\partial T} \tag{3}$$

with p the true pyroelectric coefficient = $\partial P_s/\partial T$. If a constant electric field is applied to the pyroelectric device, then one must consider the temperature dependence of the permittivity, which can be considerable in the case of ferroelectrics that constitute the main pyroelectric materials applied today. However, in the absence of a bias electric field, which is the usual operation of a pyroelectric device, p_g reduces to p.

For a ferroelectric pyroelectric to operate as an IR-sensor or energy harvester, a poling treatment is necessary to orient the ferroelectric domains. This is usually done by applying an electric field higher than the coercive field across the electroded device, which is normally a plate capacitor, as seen in Figure 1. A high coercive field and moderate operating temperature—with respect to the transition/curie temperature—ensure stable polarization and a high resistance to depolarization. In this configuration, the pyroelectric coefficient p (C/m^2K) is treated as a scalar.

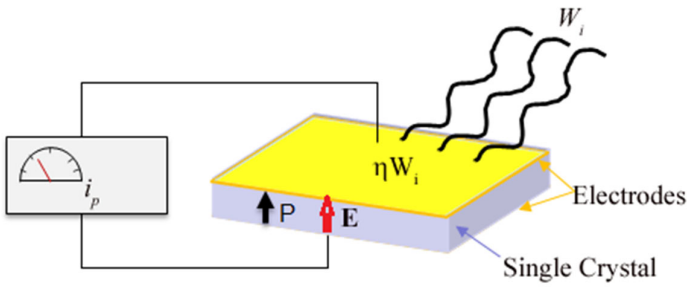

Figure 1. Schematic of a pyroelectric single crystal with bottom and top electrodes (yellowed); poling with an electric field, E, along the thickness direction results in a net polarization P parallel to E. A periodically changing incident heat wave W_i, absorbed at the fraction ηW_i, where η is the emissivity of the surface, leads to a ΔT increase of the temperature of the crystal. Owing to the pyroelectric effect, this results in an electric charge, ΔQ, collected at the electrode surface.

A periodically changing incident heat wave/IR-radiation with a power density W_i/A is absorbed by the pyroelectric device at a fraction ηWi, where $\eta \leq 1$ is the emissivity of the surface (η can be maximized by taking advantage of special absorber coatings). The temperature of the device will then rise by dT. Assuming that the power is rapidly absorbed through its volume, Equation (4) holds [4]:

$$\eta W_i dt = HdT = \varrho cAhdT \tag{4}$$

where $H = \rho cAh$ is the heat capacity of the device, ρ is the density, c is the specific heat capacity, h is the thickness, and A is the area of the pyroelectric device. The increase in dT of the temperature of the unclamped, stress-free pyroelectric results in a net charge

$$dQ = AdP_s = ApdT \tag{5}$$

collected on the electrode surface. Rearranging (4) and (5) yields:

$$i_p = \frac{\eta W_i}{\varrho ch} p \tag{6}$$

where i_p is the pyroelectric current. For an ideal capacitor, the maximum electrical power, W_0, generated is $W_0 = Vi_p$, where V is the electric potential given by Equation (7), in which C is the capacity, $\varepsilon^{33} (= \varepsilon_0 \varepsilon_r^{33})$ the permittivity in the thickness/polar direction, ε_0 the permittivity of free space, ε_r^{33} the relative dielectric constant, and $c' = \rho c$ the volume specific heat (in J/m^3K).

$$V = \frac{\Delta Q}{C} = \frac{pA\Delta T}{C};\ C = \frac{A\varepsilon^{33}}{h} \rightarrow V = \frac{p\Delta Th}{\varepsilon^{33}} \tag{7}$$

which yields a maximum electrical power of:

$$W_0 = \eta W_i \frac{p^2}{\varrho c \varepsilon^{33}} \Delta T = \eta W_i \frac{p^2}{c' \varepsilon_0 \varepsilon_r^{33}} \Delta T \tag{8}$$

For a given absorbed power, associated with a temperature rise ΔT of the device, the generated electrical power W_0 is maximized when the

$$\text{FOM} - W_0 = \frac{p^2}{\varrho c \varepsilon^{33}} \text{ in } K^{-1} \tag{9}$$

is maximized, meaning that materials with high pyroelectric coefficients, low dielectric constants, and low volume specific heat are best suited for energy harvesting.

Similarly to the FOM of thermoelectric energy harvesters [3], one may multiply FOM$-W_0$ with ΔT to obtain a slightly modified FOM$-W_0'$:

$$\text{FOM} - W_0 = \frac{p^2}{\varrho c \varepsilon^{33}} \Delta T \tag{10}$$

where ΔT is the temperature amplitude of the heat wave or the temperature difference between the heat source and heat sink.

Alternative FOMs have been suggested by others (see [5] for a review). In particular, a FOM related to the stored energy in a capacitor ($\text{FOM}' = \frac{p^2}{\varepsilon_0 \varepsilon_r^{33} c'^2}$) has been derived. Nevertheless, the FOM$-W_0$ expressed in Equation (10) specifically relates to the generated electrical power upon heat absorption, causing a temperature rise of ΔT, and is thought to describe more practically pyroelectric energy harvesting devices.

2. Experiment

For the present study, 0.3 at.% Mn-doped PMN-PT and PIN-PMN-PT single crystals, grown using a modified Bridgman technique, were purchased from different suppliers. The as-grown single crystals were oriented along <111> (the orientation is indexed as pseudo cubic phase). Grinding and polishing to different thicknesses was conducted using a custom-made polishing machine with controlled applied force of some newtons in order to ensure no damage to the crystals. For electrical measurements, gold electrodes were printed on the top and bottom surfaces of the samples. The crystal chips were eventually annealed in air to heal defects (see main text). In some experiments, the crystals were cooled under an electric field to stabilize domain structure. The dielectric properties were measured as a function of temperature at 1 kHz, 10 kHz, and 100 kHz, and a heating rate of 3 °C/min using a computer-controlled impedance analyzer (Agilent4192A, Santa Clara, CA, USA). The *P-E* hysteresis loops were measured with a ferroelectric tester (TF Analyzer 2000, AIXaCt, Aachen, Germany) at a test frequency of 10 Hz. The pyroelectric properties were measured using a custom set-up, as indicated in the main text. Domain imaging (non-quantitative) was performed after removing the gold electrodes using a fluorescence microscope (Axio, Carl Zeiss, Jena, Germany).

3. Results and Discussion

3.1. PMN-PT-Based Single Crystals for Pyroelectric Energy Harvesting

Single crystals of $(1-x)(Pb(Mg_{1/3}Nb_{2/3})O_3–xPbTiO_3$ (PMN-PT) have emerged in the last decade as highly promising multifunctional materials with excellent electromechanical and electrooptical properties, particularly for compositions close to the morphotropic phase boundary (MPB) [7], as seen in Figure S1 (Supplementary Online Information).

Excellent pyroelectric properties were reported for Mn-doped, <111> oriented PMN-PT single crystals with PT concentrations in the vicinity of MPB [8,9]. My own investigations into the structure and phase transition of PMN-29 PT had shown that the crystal undergoes complex phase transition sequences depending on temperature and poling [10]. Specifically, unpoled rhombohedral crystals, upon poling, undergo a phase transition to a monoclinic M_A phase that transforms at 100 °C to the monoclinic M_C phase, further to the tetragonal phase (T) at 110 °C, and the cubic phase (C) at 124 °C (Figure 2).

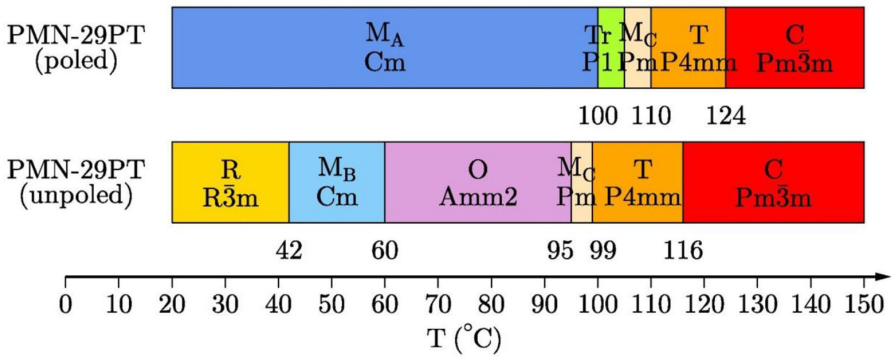

Figure 2. The sequences of phase transformations in unpoled and poled <111> oriented PMN-29PT single crystal (see [10] for more detail).

Temperatures in the lower range of 100 °C, where the first phase transformation occurs, must be regarded as the maximum operating temperatures of devices based on these crystals, as above this temperature, depolarization takes place. Lower crystal PT contents, e.g., as in PMN-28PT, are characterized by even lower transition temperatures, as shown in Figure 3.

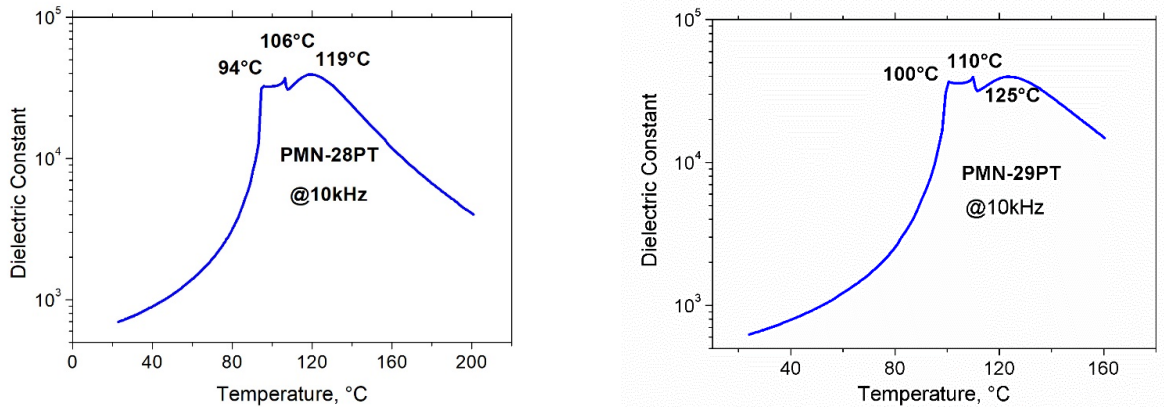

Figure 3. The temperature dependence of the dielectric constant of poled crystals, showing the dielectric anomalies at the temperature indicated for the MA → MC → T → C.

The pyroelectric and dielectric properties are also very much dependent on PT content, as illustrated in Table 1. As it appears, the FOMs calculated using Equation (9) are substantially higher for the PMN-PT single crystals in comparison to the FOM of the conventional pyroelectric $LiTaO_3$ single crystal material. However, one may also note the importance of the dielectric constant in determining the magnitude of the FOM. Although the pyroelectric coefficient of PMN-27PT is higher than that of PMN-28PT, the FOM of the latter is slightly higher because of its lower dielectric constant. A moderate decrease in the pyroelectric coefficient together with a moderate increase in the dielectric constant, as in the case of PMN-29PT and PMN-30PT, results in a substantial depression of the FOM.

The PMN-PT single crystals described above are certainly not suitable for operational temperatures higher than their initial transition temperatures (see Figure 3), while the $LiTaO_3$ single crystal, with its T_C of 650 °C, presents stable polarization at temperatures above 300 °C, which constitute an important temperature level in industrial waste heat generation [11]. However, PMN-28PT or PMN-29PT may be advantageously used to operate self-powered IoT devices in air-cooled data centers, where exhaust air temperatures [12] have been shown to be in the range of 40 °C.

Table 1. Room-temperature properties of <111> oriented PMN-PT single crystals with different PT contents in comparison to those of the conventional pyroelectric $LiTaO_3$ single crystal. The pyroelectric coefficient was obtained using the experimental set-up described in references [13,14]. The temperature of the Peltier-element was modulated at 25 mHz with an amplitude of 0.5 K. For the FOM-calculation: c' (PMN-PT)[8] = 2.510^6 J/Km^3; c' ($LiTaO_3$) = 3.210^6 J/Km^3 [4]; * own measurement under the conditions above.

Material	p, C/m^{2}K 10^{-6}	ε_r (1 kHz)	FOM$-W_0$ K$^{-1} \times 10^{-6}$	FOM′ (m^{3}J^{-1}) 10^{-11}
PMN-27PT	1100	580	94.3	3.77
PMN-28PT	1080	550	95.85	3.83
PMN-29PT	1030	605	79.25	3.17
PMN-30PT	980	650	66.80	2.67
$LiTaO^3$	176 *	44	24.85	0.77

3.2. <111> PIN-PMN-PT Single Crystals as Promising Alternative to PMN-PT

Equations (8) and (10) show that the harvested electrical power and FOM depend on the temperature rise ΔT of the device. As stated above, the transition temperature of PMN-PT single crystals is relatively low, which imposes an operating temperature < 100 °C to avoid depolarization. To increase the transition temperature, and in so doing widen the temperature range of the harvesting device, several strategies were undertaken. The most promising among them was the development of ternary single crystal systems based on the

stoichiometry x-Pb($In_{1/2}$ $Nb_{1/2}$)O_3-y-Pb($Mg_{1/3}$ $Nb_{2/3}$)O_3-(1 − x − y)-$PbTiO_3$ (PIN-PMN-PT). These systems have been shown to possess higher transition temperatures, together with high pyroelectric properties. Acceptor doping with Mn resulted in depression of the dielectric constant and the dielectric loss and an improvement in the ferroelectric properties (higher coercive field and remnant polarization). In the following sections, the results obtained for several stoichiometries that are outlined in the ternary phase diagram [15], Figure 4, are presented.

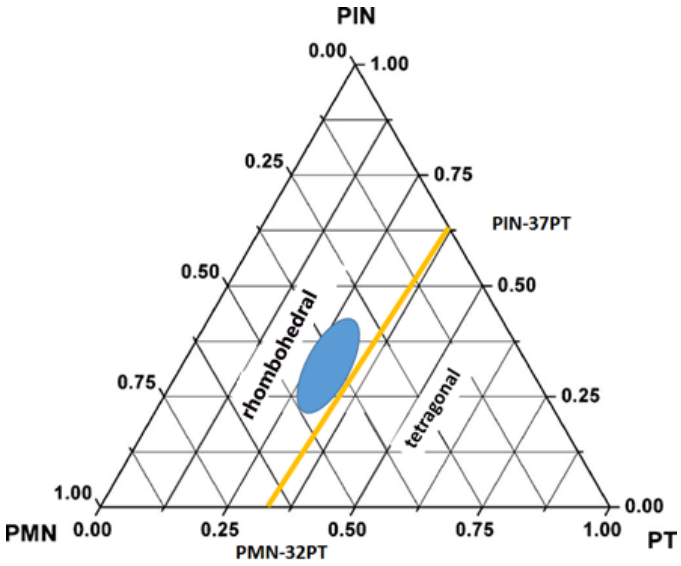

Figure 4. Ternary PIN-PMN-PT phase diagram after D. Wang, et al. [15]. The locus of the morphotropic phase boundary (MPB) is indicated by the yellow line. The selected compositions near the MPB investigated in this work are inside the blue area. A tetragonal [001] PMN-37PT was also evaluated for comparison. The ternary phase diagram is reprinted from Wang, D.; Cao, M.; Zhang, S. Phase diagram and properties of $Pb(In_{1/2}Nb_{1/2})O_3$–$Pb(Mg_{1/3}Nb_{2/3})O_3$– $PbTiO_3$ polycrystalline ceramics. J. Eur. Cer. Soc., 2012, 32, 434, © Elsevier 2011, with permission from Elsevier.

The temperature dependence of the dielectric properties is shown in an exemplary manner in Figure 5, and Table 2 lists the values of the transition temperatures together with the dielectric properties, the pyroelectric coefficients at room temperature, and the FOMs. Figure 6 shows the temperature dependence of the pyroelectric coefficient of PIN-PMN-PT:Mn in comparison to PMN-29PT.

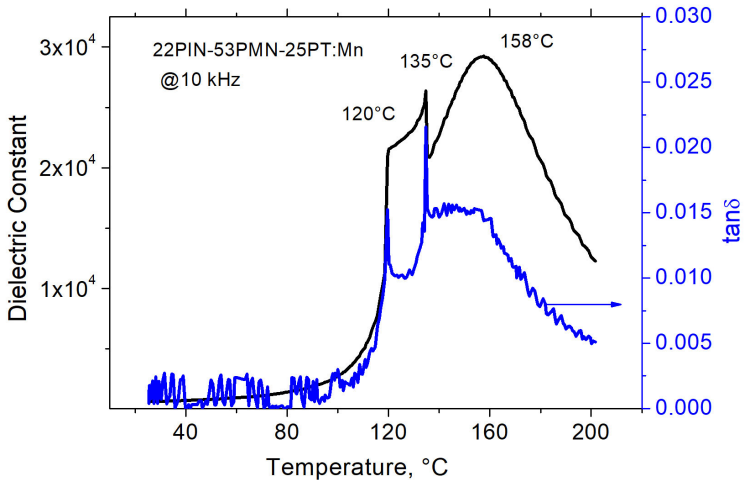

Figure 5. The temperature dependence of the dielectric constant and the loss-tangent of <111> 22 PIN-53 PMN-33 PT:Mn single crystal, showing the dielectric anomalies at the phase transition temperatures.

Table 2. The different <111> PIN-PMN-PT single crystals investigated in terms of their transition temperatures, pyroelectric coefficients, dielectric constants, and FOM-W_0. The properties of the tetragonal [001] PMN-37PT and <111> PMN-29PT crystals are also indicated for comparison.

Single Crystal Stoichiometry	T_{R-T}, °C	T_c, °C	p, 10^{-6} C/m^{2}K	ε_r	FOM$-W_0$, 10^{-6}K^{-1}
32PIN-42PMN-27PT:Mn	131	172	770	530	48.7
22PIN-53PMN-25PT:Mn	120	158	910	543	68.9
25PIN-42PMN-32PT:Mn	121	170	788	514	51.7
PMN-37PT (tetragonal)	-	145	650	769	24.8
PMN-29PT	100	124	1030	605	79.25

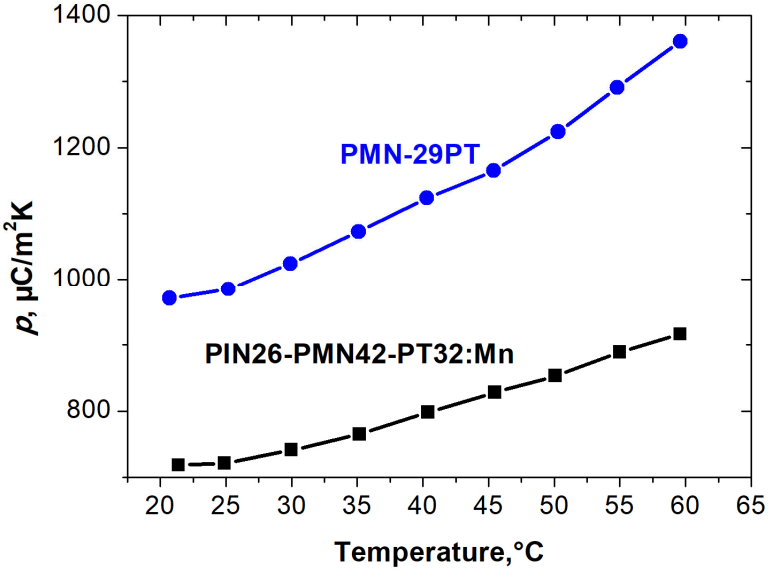

Figure 6. The temperature dependence of the pyroelectric coefficient of a PIN-PMN-PT:Mn single crystal in comparison to PMN-29PT. The slopes are approximately 12 (μC/m^{2}K)/K for PMN-29PT and 5 (μC/m^{2}K)/K for PIN-PMN-PT:Mn.

Table 2 shows that all the ternary crystals have a higher transition temperature than the binary crystals, which has the merit to extend the operating temperatures of the energy harvesting devices. This, however, happens at the expense of the pyroelectric properties and the FOM-W_0. Nevertheless, the 22PIN-53-PMN-25Pt:Mn crystal slightly overrides the FOM of the PMN-30PT crystal (see Table 1) while extending the transition temperature by approximately 20 °C. The tetragonal PMN-37PT crystal shows the same FOM as $LiTaO_3$, but with the disadvantages of the brittleness inherent to the tetragonal composition and the much lower transition temperature. Therefore, the application of these tetragonal crystals alone to pyroelectric energy harvesting devices can be judged to be of no benefit. However, it might be useful if one combines both pyroelectric and piezoelectric energy harvesting, since [001] oriented tetragonal crystals show outstanding piezoelectric properties [16].

The temperature dependence of the pyroelectric coefficient is displayed in Figure 7 for temperatures up to 60 °C. The binary crystals exhibit a higher slope than the ternary crystals because of their lower transition temperature (the pyroelectric coefficient is at its maximum in the vicinity of the transition temperature). It should then be expected that the FOM also increases, but the increase in temperature is also accompanied by an increase in the dielectric constant, with an approximate slope (the temperature coefficient of the dielectric constant) of 8.7 K^{-1}. This should mitigate or even lessen the FOMs, as illustrated in the following example: we compare the FOMs of 25PIN-42PMN-32PT and PMN-29PT at 50 °C; for the former p = 853 μC/m^{2}K, ε_r = 765, and the latter p = 1224 μC/m^{2}K, ε_r = 956, which

yields FOMs of 42 × 10^{-6} K^{-1} and 70 × 10^{-6} K^{-1}, respectively (both FOMS are smaller than the FOMs at room temperature). Furthermore, in the absence of an electric field, higher operation temperatures, particularly in the vicinity of the transition temperature, lead to depolarization of the pyroelectric material (see below).

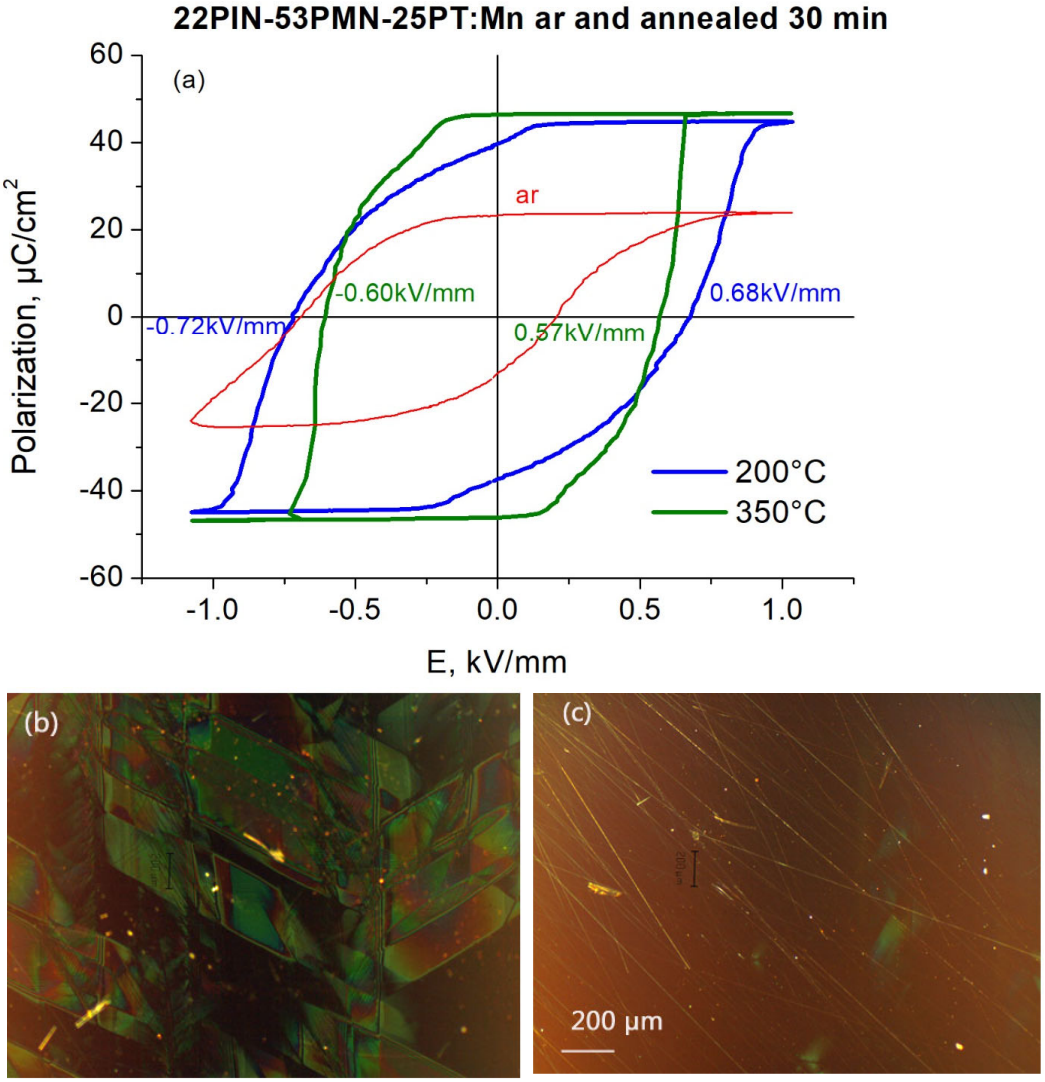

Figure 7. (**a**) Polarization-E field hysteresis loops of a Mn-doped <111> PIN-PMN-Pt single crystal in the as-received (ar) poled state, and post-heat treatment at two different temperatures above T_c, (**b**) a polarization microscope image showing the domain state of the as-received crystal, and (**c**) after post heat treatment at 350 °C and subsequent poling at 80 °C, followed by field cooling to room temperature. The magnification is the same for both Figures.

3.3. Technological Aspects: The Effects of Domain Structure, Poling Conditions and Thickness on the Properties of PMN-PT Base Crystals

3.3.1. Effects of Domain State and Poling Conditions

In previous work, we have shown that the domain structure substantially impacts the dielectric and pyroelectric properties of <111> PMN-28PT single crystals. In particular, a poling treatment that results in a single domain structure had the benefits of a lower dielectric constant and dielectric loss and a higher pyroelectric coefficient [17]. These results also apply to the more complex PIN-PMN-PT:Mn system. A 250 μm thick <111> 22PIN-53PMN-25PT:Mn crystal in the as-received poled state shows coarse stripe domains and a rather deformed hysteresis loop, as seen in Figure 7. However, the properties can be substantially improved via annealing at temperatures above T_c, which is expected to

heal out surface defects and drastically decrease residual stresses (provided that slow heating and cooling rates are applied). Subsequent re-poling either at room temperature or at temperatures below the first transition temperature generally changes the domain state to an almost monodomain state (see Figure 7c), thus minimizing the contribution of domain walls to permittivity, and consequently positively impacting both the dielectric and pyroelectric properties, and through them the FOM. Table 3 lists the properties obtained before and after post-treatment and repoling.

Table 3. The dielectric, pyroelectric, and FOM properties of 22PIN-53PMN-25PT:Mn in different treatment states.

Property	As-Received	Repoled at RT	Repoled at 80 °C
ε_r	600	560	543
tanδ	0.0017	0.0015	0.0013
p, $\mu C/m^2K$	845	887	910
FOM$-W_0$, $10^{-6}K^{-1}$	53.8	63.5	68.9

The properties may, however, be subject to large scatter, depending on the domain state of the crystal which in turn is liable to its treatment and stress history. Table 4 gives an account of this fact in the case of two chips of the same <111> 25PIN-42PMN-33PT:Mn crystal, diced each in 3 samples, electroded, and poled at room temperature under the same conditions (1 kV/mm). Polarization microscopy images of the domain states of the samples, as well as the corresponding high-resolution XRD patterns, are shown in Figures S2 and S3 (supplementary information).

Table 4. Dielectric and pyroelectric properties of <111> 25PIN-42PMN-33PT:Mn crystal samples with different domain states. These are <111> domains, qualitatively assessed in their density (see also Figure S2 (Supplementary Information)) and reference [17].

	ε_r	$tan\Delta$	p, $\mu C/m^2K$	Domain State *
Sample-1a	542	0.0025	767	Few stripe domains
Sample-1b	574	0.0025	765	More domains
Sample-1c	632	0.003	727	Many more domains
Sample-2a	514	0.0022	788	Very few domains at sample edge
Sample-2b	705	0.0033	706	Many more domains
Sample-2c	674	0.0034	685	Many more domains

* see Figure S2.

It appears that the samples exhibiting a multidomain state contain different amounts of metastable phases that are manifested through a slight shift of the 2Θ position of the 222 reflection with respect to the reflection pertaining to the sample in the monodomain state, and the observation of an additional reflection at higher 2Θ (Figure S3). It follows that the multidomain state and the related metastable phases are a consequence of a non-optimal poling [18]. Most probably, surface and bulk defects, as they may arise from dicing and presumably compositional fluctuation during crystal growth, together with dipolar $(Mn'' - V_O^{\cdot\cdot})$ defects (see below) and residual stresses are responsible for domain pinning effects. These phenomena are expected to impact the poling efficiency and consequently the functional properties. Fortunately, as described below, it is possible to attain a narrow scatter band for the properties through appropriate post-heat treatment and poling sequences, which should result in pyroelectric harvesting devices with more reliable properties.

3.3.2. Thickness Effects

Equation (6) shows that the pyroelectric current depends on the reciprocal of the thickness which means that, for a given absorbed heat, thinner crystals generate higher electrical power. This, together with higher thermal conductance and lower heat capacitance, are indisputable arguments in favor of thinner devices.

Mechanical thinning of the crystals through grinding and polishing proved, however, to be rather challenging owing to conflicting properties: the PMN-PT crystals were soft, and at the same time brittle, which demanded extra care in handling them. Further, polishing a crystal from 300 µm down to 50 µm substantially altered the properties, as shown in Figure 8 which represents the case of PMN-29PT. Restoring the properties necessitated a post heat treatment, preferably at temperatures between 350 and 500 °C to heal out surface defects introduced during mechanical handling. Repoling the crystal resulted in full recovery or even better properties, as seen in Figure 9. Additional heating and repoling sequences resulted in structure and property stabilization.

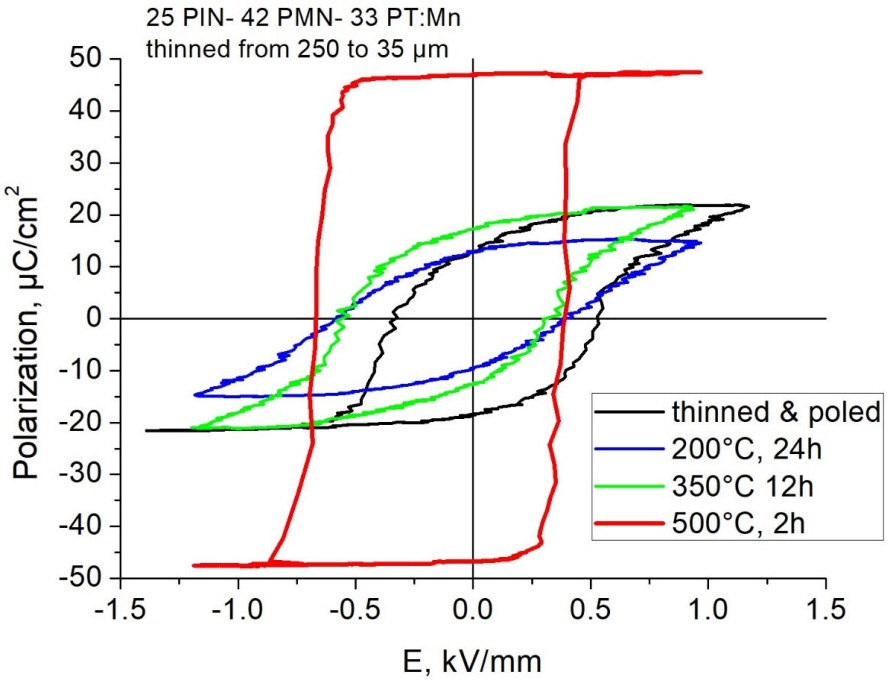

Figure 8. The P-E hysteresis loops of a PIN-PMN-PT crystal mechanically thinned from 250 µm down to 35 µm before and after heat treatment at the indicated temperatures. Heat treatment was performed in the furnace in air for the times indicated under open circuit conditions. Slow heating and cooling rates of 2 K/min were set to minimize residual stresses.

The thinning process has the same effect on the polarization and pyroelectric properties of the ternary PIN-PMN-PT crystals. Figure 9 shows the *P-E* hysteresis loops of a crystal thinned down to 35 µm before and after annealing at different temperatures. A large polarization suppression can be observed for the thinned, non-heat-treated crystal. Even 30 min of treatment at 350 °C scarcely changes the shape of the hysteresis loop, and a higher heat-treatment temperature of 500 °C is necessary to fully restore the polarization properties. However, as Figure 8 clearly shows, an important built-in internal bias field can be noted in this state, which may explain the ageing behavior described below.

Table 5 lists the properties obtained for the crystals thinned and subsequently annealed at two different temperatures, followed by poling. As can be seen, the FOM substantially increases upon annealing at 500 °C for at least 2 h, which has proved necessary to minimize the impact of surface defects on the crystal properties.

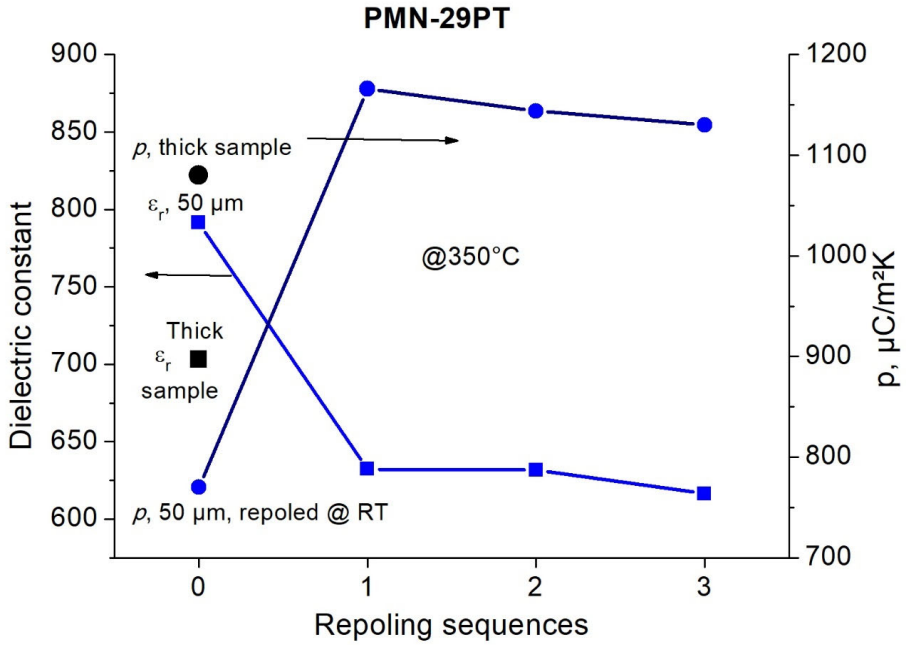

Figure 9. Comparison of the properties of 300 μm thick PMN-29PT crystal (black symbols) and the same crystal when thinned down to 50 μm. Sequences of ageing at 350 °C for 30 min, cooling, and repoling restored the pyroelectric property while decreasing the dielectric constant (square symbols represent the dielectric constant).

Table 5. Properties of a <111> 25PIN-42-PMN-33PT:Mn crystal chip thinned from 250 μm down to 35 μm, annealed at two different temperatures and repoled after cooling (see Figure 10 above).

Property	Annealed @ 350 °C, Repoled @ RT	Annealed @ 500 °C, Repoled @ RT
εr	700	550
$tan\delta$	0.004	0.0015
p, $\mu C/m^2K$	650	780
FOM$-W_0$, $10^{-6}K^{-1}$	27.3	50.0

Crystal thinning and necessary subsequent treatments all add to the costs incurred in the fabrication of a harvesting device. This may shift interest to thin films, and indeed, some published work had shown that PMN-PT relaxor thin films may be very well suited for pyroelectric energy harvesting. Pandya et al. [19] reported on a heterostructure of 150 nm PMN–0.32PT/20 nm $Ba_{0.5}Sr_{0.5}RuO_3$/on (110) $NdScO_3$ obtained via laser ablation which, they claim, exhibited the best power density and efficiency ever measured, taking advantage of the Ericsson cycle under a field of 271 kV/cm. Furthermore, the clamped structure benefited from dielectric suppression in high dc electric fields. However, the film was eventually operated above the transition temperature from the monoclinic to the cubic phase, and considering the high applied electric fields, the issue of conductivity is all the more urgent to examine. While these results were very encouraging, the shortcomings of such structures should not be ignored. Particularly, the power dissipated in the dielectric thin film, which depends on the dielectric loss (tanδ is at best 0.02), the frequency of the electric field, and repeated heating should at some time compromise the structural stability of the thin film. Based on these considerations, there are good reasons to question the durability of systems based on thin films, and optimally thinned single crystals constitute the better choice, in the opinion of this author.

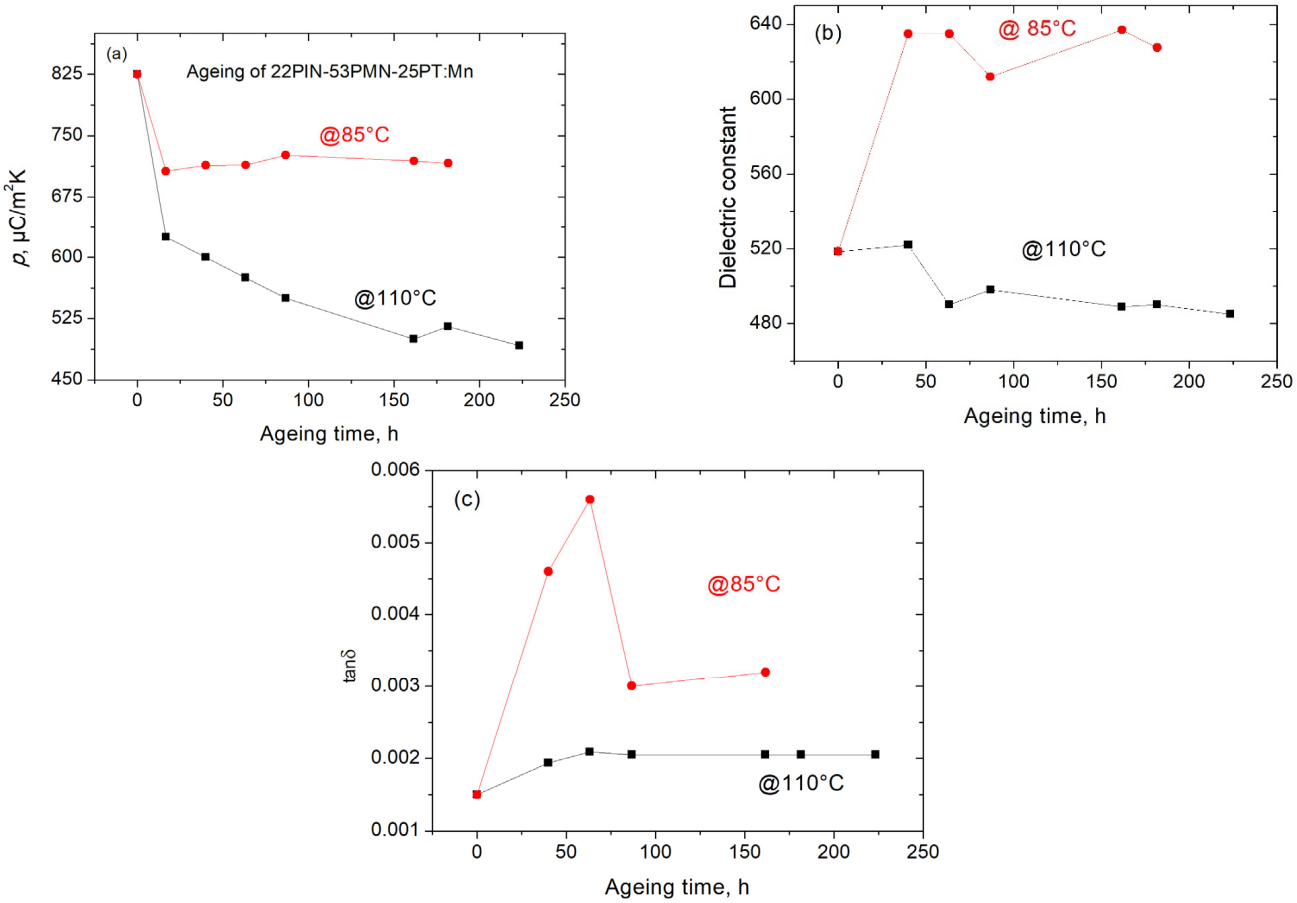

Figure 10. Ageing of a <111> 22PIN-53PMN-25PT crystal at 85 and 110 °C under open circuit conditions. (**a**) The evolution of the pyroelectric coefficient with the ageing time, (**b**) that of the dielectric constant, and (**c**) that of the loss tangent, tanδ, at 10 kHz. The lines are a guide for the eye. Note that the measurements were performed after cooling the crystal to room temperature. Note also that the measurements were performed on a heat-treated and poled 50 μm thin crystal sample.

3.3.3. Ageing Effects

As pointed out above, operating pyroelectric energy harvesting devices at temperatures near the transition temperature is expected to depolarize the material and consequently decrease the FOM. In the following, preliminary ageing experiments are presented with emphasis on the effects on the pyroelectric coefficient and dielectric constant. Figure 10 illustrates how ageing at two different temperatures of 85 °C and 110 °C (the latter is 10 °C below the T_{R-T} (see Table 2)) affected these properties. Figure 10a shows that for both ageing temperatures, a steep decrease in the pyroelectric coefficient was observed after 24 h ageing. For longer ageing times, temperature specific behavior was noted: at 85°, the pyroelectric coefficient experienced a slight increase during longer ageing times (probably because depolarization is somewhat counterbalanced by the increase in the pyroelectric coefficient with temperature, see Figure 6). At 110 °C, however, a regime of constant, gentle decrease for as long as 150 h ageing was observed, followed by stabilization of the property above this time to a value that is almost half that of the pristine sample. Similar behavior was observed for the dielectric constant at 110 °C upon ageing for 50 h, although the property decrease was not as steep as that of the pyroelectric coefficient, as represented in Figure 10b. This was accompanied by an almost constant loss tangent, tanδ, (Figure 10c). However, a completely different picture of the dielectric constant and tanδ was revealed after ageing at 85 °C; a leap in the dielectric constant of approximately 26% was observed after the first hours of ageing, followed by saturation at values around 620. This was accompanied by a

leap in tanδ values that, however, decreased over a longer ageing time, but remained higher than the values obtained at 110 °C for the same ageing time (see below for discussion).

Depolarization and ageing of PMN-PT base crystals with and without a bias field, at temperatures near or above the transition temperature were reported in early work, although mostly in relation to piezoelectric applications [20–22].

Generally, the phenomenon of the ageing of ferroelectrics has been widely addressed in the literature, and a detailed account of the mechanisms may be found in the review article by Genenko et al. [23]. However, as pointed out in reference [20], PMN-PT relaxor single crystals behave differently upon ageing owing to their specific microdomain structure; others have stressed the importance of defects [24,25], particularly in acceptor-doped PMN-PT-base crystals. The ageing of the piezoelectric and pyroelectric properties of PMN-PT base crystals depends on the ageing temperature, as shown in Figure 10a for the pyroelectric coefficient, and is in this respect a thermally activated process. Further, the magnitude of the built-in internal field associated with defects is critical to the severity of the depolarization processes [20,22]. For the PIN-PMN-PT:Mn single crystals investigated here, e.g., Figure 10, the concentration of defects, and consequently the magnitude of the defect field, e.g., Figure 9, are expected to be roughly the same, which begs the question as to why the ageing behavior of the dielectric constant at 85 °C is opposite to that at 110° C. At this stage, and until more elaborated ageing experiments are available, the following mechanism might apply: at 85 °C, depolarization might be responsible for the flipping of the 1R monodomain state to a multidomain state (Figures S2 and S3), and/or the growth of those domains already existent in the poled state at room temperature. Further, it is surmised that oxygen vacancy diffusion is sluggish at 85 °C owing to a low driving force at this temperature (the activation energy for the diffusion of oxygen vacancies in Mn-doped crystals is reported to be roughly 1 eV [26]; this yields a diffusion coefficient roughly 0.15 times the diffusion coefficient at 110 °C). Consequently, the domain structure is not stabilized via the segregation of dipolar defects to domain walls, and this in turn would lead to a large domain wall contribution to the dielectric constant and dielectric loss. This is factually what Figure 10b,c reflect. Continuing this path of reasoning, it can be said that at 110 °C the diffusion kinetics of the oxygen vacancies—which are roughly seven times higher than at 85 °C—readily lead to the formation of defect dipoles at the domain walls, thus stabilizing them, and resulting in a lower dielectric constant as ageing proceeds. The slight increase in the dielectric constant and loss tangent at the beginning of ageing is an argument in favor of the proposed mechanism, as diffusion is time limited.

These ageing experiments appeal to some comments as to the performance of PIN-PMN-PT single crystals in harvesting devices that are operated at temperatures fluctuating at around 100 °C, without the application of an external electric field. If we compare the FOMs after a long period of ageing, say 200 h, at 85 and 110 °C, the values obtained are 37×10^{-6} K^{-1} and 24.7×10^{-6} K^{-1}, respectively. These are rather sobering results, as these crystals, at least those that are now available, afford higher advantages over $LiTaO_3$ (FOM of 24.85×10^{-6} K^{-1}) only when they are operated at temperatures lower than 100 °C. As pointed out earlier, a possible application of harvesting devices based on PIN-PMN-PT is in air cooled data centers and in some sectors that generate industrial waste heat [11]. At higher temperatures, $LiTaO_3$ or a pyroelectric ceramic with higher T_c are more advantageous because of their higher transition temperatures and property stability in a wide temperature range. Another picture is revealed if one operates the device under an Ericson/Olsen cycle with an applied electric field in the range of the coercive field (see below). In this case, the device may be operated at temperatures up to the transition temperature, with efficiencies higher than any other pyroelectric.

3.4. Perspectives in Materials and Process Development

Single crystal material development for pyroelectric applications is rather sluggish because of the relatively small market in comparison to the much bigger market for piezoelectric sensors and actuators. One system that has undergone preliminary investigation

in this work is the PMN-PZ-PT system, which has proved to be promising, in particular in regard to its higher transition temperature together with its pyroelectric properties, which are similar to those of PIN-PMN-PT:Mn crystals. Figure 11a shows the temperature dependence of the dielectric constant of a single crystal with the 0.48Pb($Mg_{1/3}$ $Nb_{2/3}$)O_3-0.16$PbZrO_3$-0.36$PbTiO_3$ stoichiometry. The T_{R-T} transition temperature of 137 °C is already satisfactory, but may be improved, provided the crystal chemistry is optimized. The ferroelectric properties are outstanding, as demonstrated in Figure 11b.

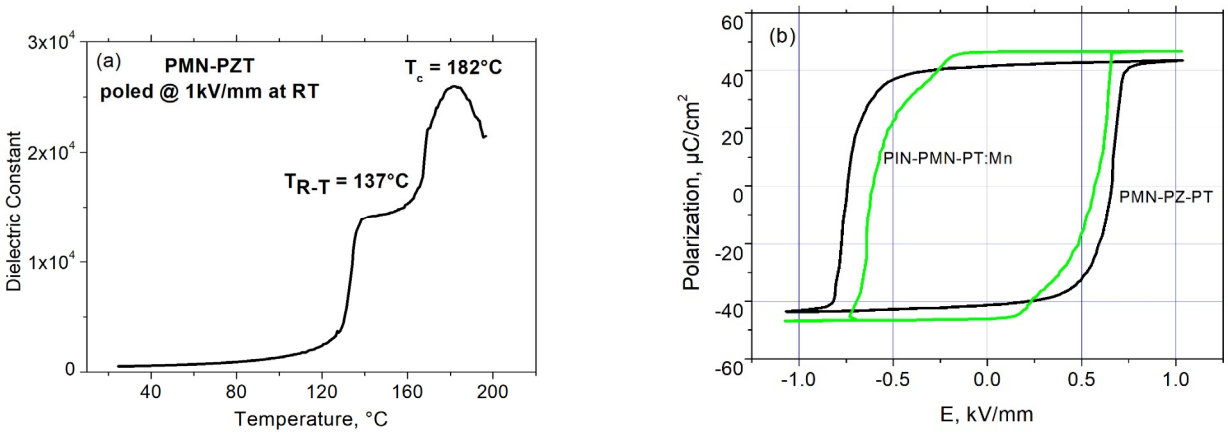

Figure 11. The temperature dependence of the dielectric constant of a PMN-PZ-PT single crystal, annealed and subsequently poled at room temperature (**a**), and (**b**) the P-E hysteresis loop of the same crystal in comparison to that of PIN-PMN-PT:Mn, both in the annealed state. Notice the well-shaped hysteresis loop and the larger coercive field of PMN-PZ-PT crystal.

Table 6 shows the properties obtained for two PMN-PZ-PT crystal samples in comparison to PIN-PMN-PT:Mn. While the FOM$-W_0$ of the former is smaller, its operation temperature range is extended, which if Equation (13) holds could result in better device performance (see below).

Table 6. The properties and FOM$-W_0$ of two 48PMN-16PZ-36PT single crystal samples in comparison to a PIN-PMN-PT:Mn crystal (see Table 4).

Property	Sample 1, Annealed, Poled at RT	Sample 2, Annealed, Poled at RT	25PIN-42-PMN-33PT:Mn Repoled at 80 °C
ε_r	484	497	543
$tan\delta$	0.0043	0.0032	0.0013
p, $\mu C/m^2K$	727	744	910
FOM$-W_0$, 10^{-6} K^{-1}	49.4	50.4	68.9

Beyond materials development, process optimization may also lead to an extended operational temperature range and better properties. In particular, thinner crystals, if mounted on high thermal expansion substrate, e.g., an austenitic stainless-steel substrate, may show a reduced dielectric constant and higher pyroelectric coefficient together with a higher transition temperature, mediated by high induced tensile stress in the crystal [14,27].

3.5. Pyroelectric Energy Harvesters Based on PMN-PT Single Crystals

The operation of a pyroelectric energy harvester, like that of a pyroelectric detector, is liable to periodically varying or pulsating incident heat power. In this respect, the collected pyroelectric current will depend on the frequency of the incident power wave [4]. A quasi-stationary or a low-frequency heat wave will thus result in low power output. However, as has been shown in earlier work where different cycle types were investigated [28], the

power output may be substantially improved if an electric-Ericson/Olson cycle is adopted. As illustrated in Figure 12, the pyroelectric material is electrically cycled between a cold and a hot isotherm. As described by Hunter et al. [29] and Pandya et al. [19,30], the cycle starts at one by heating the poled pyroelectric from a low temperature, T_L, to a high temperature, T_H, under a constant electric field, E_1, which, owing to the pyroelectric effect, releases electric power and at the same time charges the capacitor. At two, the electric field is then isothermally decreased to E2, leading to partial depolarization of the pyroelectric, and at three, the pyroelectric temperature is isoelectrically decreased to T_0, which leads to inverse charge and release of power. From four to one, the capacitor is once more polarized, and the cycle can start again.

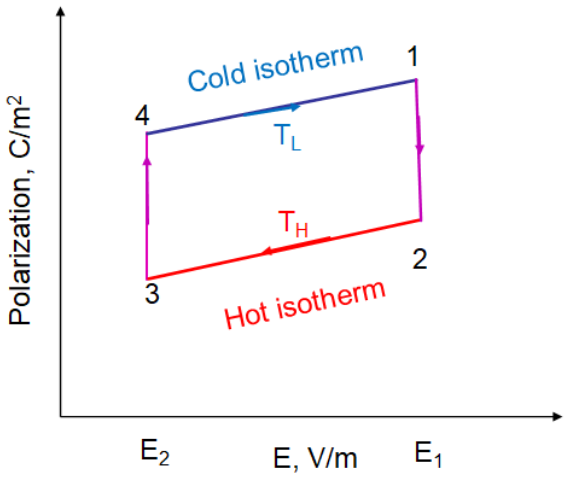

Figure 12. The Ericson-Olson cycle, showing 1 cycle starting at the cold isotherm 1 with the poled pyroelectric at a temperature T_L and an applied electric field E_1 (see the text for more details).

It has been shown that the Ericson/Olson cycle may lead to substantially higher power output [28–30]. Using Equation (6), the pyroelectric current is given by:

$$i_p = Ap\frac{dT}{dt} \tag{11}$$

However, because an electric field (E_1-E_2) is applied, the second term in Equation (3) can no longer be ignored, and the generalized pyroelectric coefficient, p_g, must be considered. The net power can then be expressed as:

$$W = (V_1 - V_2)i_p = \Delta VAp_g\frac{dT}{dt} \tag{12}$$

Ignoring the piezoelectric contribution from the thermal expansion of the pyroelectric, the total power for one cycle is given by:

$$W_T = \oint EdP = \int Wdt = \Delta VA\int p_g\frac{dT}{dt}dt \tag{13}$$

However, a real dielectric is subjected to dielectric loss, $tan\partial$, that entails a dissipated power, W_d, given by Equation (14):

$$W_d = 2\pi f tan\partial W_T \tag{14}$$

where f is the frequency of the applied electric field. A low $tan\partial$ is therefore a further requirement for a good pyroelectric harvester.

Equation (13) has different implications: first, cycling the pyroelectric at a high rate would result in high power output, but this is usually difficult to achieve in "bulk" crystals and would require thin films (although the pyroelectric properties of thin film do not match

those of single crystals, and their dielectric properties are generally worse (high dielectric constant and high $tan\partial$). Secondly, p depends on temperature, and is at its maximum in the vicinity of the phase transition, so T_H should be high enough to approach this temperature to maximize power. Thirdly, because the electric field, E, has a finite value, the generalized pyroelectric coefficient, Equation (3), must be considered as the temperature dependence of the permittivity can be substantial in ferroelectrics, e.g., as seen in Figure 5. The main issue with the Ericson cycle lies in its necessity for the provision of an external voltage that should be high enough and stable enough to operate the harvester. For instance, for a 50 µm thick crystal, the voltage required should be in the range of 50 V (considering a coercive field of 1 kV/mm). For IoT devices, however, the coupled pyroelectric harvester may generate enough power in the presence of a periodically changing heat source, e.g., using a chopper, without the provision of an external voltage, making self-powered devices possible.

4. Conclusions

In this paper, the application of <111> PMN-PT-base single crystals for pyroelectric energy harvesting is explored from different points of view, including technological aspects such as poling, thickness effects, and ageing. These crystals exhibit some of the best pyroelectric properties among ferroelectric materials. Their main drawback, however, is their relatively low transition temperatures, which somewhat limit their operating temperature range. A figure of merit (FOM) for pyroelectric energy harvesting is first derived based on the formalism of the pyroelectric effects. The FOMs of different PMN-PT and PMN-PIN-PT chemistries are then compared with the FOM of the conventional pyroelectric $LiTaO_3$ single crystal. It is shown that the best FOMs are obtained with PMN-27PT and PMN-28PT, which are about four times the FOM of $LiTaO_3$. Further, the ternary system PIN-PMN-PT is considered because of its higher transition temperatures and thus the higher operating temperatures that can be achieved. Although this system is characterized by lower pyroelectric coefficients, it nevertheless matches the FOM of PMN-30PT for the composition 22PIN-53PMN-25PT:Mn while extending the operating temperature by approximately 20 °C. Another material system that shows promising FOM, PMN-PZ-PT, is also considered on a preliminary basis owing to its higher transition temperature. The upscaling of the crystals is shown to be somewhat arduous, as thinning the crystals for improved thermal management alters their properties and necessitates post-thermoelectrical treatments to recover these properties. Property change upon ageing of the crystals at temperatures below their transition temperatures also needs to be considered. Nevertheless, these crystals may be advantageously applied for pyroelectric energy harvesting, particularly for self-powered IoT devices in data centers and processes producing moderate waste heat. The devices may operate as an Ericson-cycle device with the provision of a sufficient voltage, or, in a periodically changing heat wave, similarly to pyroelectric detectors.

Supplementary Materials: The following supporting information can be downloaded at: https://www.mdpi.com/article/10.3390/cryst14030236/s1. Figure S1: the PMN-xPT phase diagram; Figure S2: polarization microscopy images; Figure S3: the <222> reflections corresponding to the samples in Figure S2.

Funding: This research was funded by the German Federal Ministry of Education and Research, Grant# 03FH008PX2, and the Federal Ministry of Economy and Environment, Grant # KF2448901JT9.

Data Availability Statement: The data presented in this study are available upon request from the corresponding author.

Acknowledgments: Thanks are also due to Matthias Dietze for experimental support. Thanks are due to Infratec Dresden and Haosu Luo for providing the crystals.

Conflicts of Interest: The authors declare no conflicts of interest.

References

1. Geffroy, C.; Lilley, D.; Sanchez, P.; Prasher, P.R. Techno-economic analysis of waste-heat conversion. *Joule* **2021**, *5*, 3080. [CrossRef]
2. Al-Sayyab, A.K.S.; Navarro-Esbrí, J.; Mota-Babiloni, A. Energy, exergy, and environmental (3E) analysis of a compound ejector-heat pump with low GWP refrigerants for simultaneous data center cooling and district heating. *Int. J. Refrig.* **2022**, *133*, 61. [CrossRef]
3. Champier, D. Thermoelectric generators: A review of applications. *Energy Convers Manag.* **2017**, *140*, 167. [CrossRef]
4. Moulson, A.J.; Herbert, J.M. *Electrocermaics*, 2nd ed.; John Wiley &Sons Ltd.: Chichester, UK, 2003; pp. 411–432.
5. Bowen, C.R.; Taylor, J.; LeBoulbar, E.; Zabek, D.; Chauhan, A.; Vaish, R. Pyroelectric materials and devices for energy harvesting applications. *Energy Environ. Sci.* **2014**, *7*, 3836. [CrossRef]
6. Toprak, A.; Tigli, O. Piezoelectric energy harvesting: State-of-the-art and challenges. *Appl. Phys. Rev.* **2014**, *1*, 031104. [CrossRef]
7. Noheda, B.; Cox, D.E.; Shirane, G.; Gao, J.; Ye, Z.-G. Phase diagram of the ferroelectric relaxor $(1-x)PbMg_{1/3}Nb_{2/3}O_3$-$xPbTiO_3$. *Phys. Rev. B* **2002**, *66*, 054104. [CrossRef]
8. Tang, Y.; Luo, L.; Jia, Y.; Luo, H.; Zhao, X.; Xu, H.; Lin, D.; Sun, J.; Meng, X.; Zhu, J.; et al. Mn-Doped $0.71Pb(Mg_{1/3}Nb_{2/3})O_3$–$0.29PbTiO_3$ Pyroelectric Crystals for Uncooled Infrared Focal Plane Arrays Applications. *Appl. Phys. Lett.* **2006**, *89*, 162906. [CrossRef]
9. Yu, P.; Ji, Y.; Neumann, N.; Lee, S.-G.; Luo, H.-S.; Es-Souni, M. Application of Single-Crystalline PMN–PTand PIN–PMN–PT in High Performance Pyroelectric Detectors. *IEEE Trans. Ultrason. Ferroelectr. Freq. Control* **2012**, *59*, 1983–1989. [CrossRef]
10. Katzke, H.; Dietze, M.; Lahmar, A.; Es-Souni, M.; Neumann, N.; Lee, S.G. Dielectric, ultraviolet/visible, and Raman spectroscopic investigations of the phase transition sequence in $0.71Pb(Mg_{1/3}Nb_{2/3})O_3$-$0.29PbTiO_3$ crystals. *Phys. Rev. B* **2011**, *83*, 174115. [CrossRef]
11. Papapetrou, M.; Kosmadakis, G.; Cipollina, A.; La Commare, U.; Micale, G. Industrial waste heat: Estimation of the technically available resource in the EU per industrial sector, temperature level and country. *Appl. Therm. Eng.* **2018**, *138*, 207. [CrossRef]
12. Ebrahimi, K.; Jones, G.F.; Fleischer, A.S. A review of data center cooling technology, operating conditions and the corresponding low-grade waste heat recovery opportunities. *Renew. Sustain. Energy Rev.* **2014**, *31*, 622. [CrossRef]
13. Dietze, M.; Krause, J.; Solterbeck, C.-H.; Es-Souni, M. Thick film polymer-ceramic composites for pyroelectric applications. *J. Appl. Phys.* **2007**, *101*, 054113. [CrossRef]
14. Es-Souni, M.; Kuhnke, M.; Iakovlev, S.; Solterbeck, C.H.; Piorra, A. Self-poled (Pb, Zr)TiO_3 films with improved pyroelectric properties via the use of La0.8Sr0.2MnO_3/metal substrate heterostructures. *Appl. Phys. Lett.* **2005**, *86*, 022907. [CrossRef]
15. Wang, D.; Cao, M.; Zhang, S. Phase diagram and properties of $Pb(In_{1/2}Nb_{1/2})O_3$–$Pb(Mg_{1/3}Nb_{2/3})O_3$–$PbTiO_3$ polycrystalline ceramics. *J. Eur. Ceram. Soc.* **2012**, *32*, 433. [CrossRef]
16. Li, F.; Zhang, S.; Xu, Z.; Wei, X.; Luo, J.; Shrout, T.R. Composition and phase dependence of the intrinsic and extrinsic piezoelectric activity of domain engineered $(1-x)Pb(Mg_{1/3}Nb_{2/3})O_3-xPbTiO_3$ crystals. *J. Appl. Phys.* **2010**, *108*, 034106. [CrossRef] [PubMed]
17. Dietze, M.; Katzke, H.; Es-Souni, M.; Neumann, N.; Luo, H.-S. Single domain vs. polydomain [111] $0.72Pb(Mg_{1/3}Nb_{2/3})O_3$-$0.28PbTiO_3$ single crystal. Polarization switching, dielectric and pyroelectric properties. *Appl. Phys. Lett.* **2012**, *100*, 242905. [CrossRef]
18. Rajan, K.K.; Shanthi, M.; Chang, W.S.; Jin, J.; Lim, L.C. Dielectric and piezoelectric properties of [0 0 1] and [0 1 1]-poled relaxor ferroelectric PZN–PT and PMN–PT single crystals. *Sens. Actuat. A* **2007**, *133*, 110. [CrossRef]
19. Pandya, S.; Wilbur, J.; Kim, J.; Gao, R.; Dasgupta, A.; Chris Dames, C.; Martin, L.W. Pyroelectric energy conversion with large energy and power density in relaxor ferroelectric thin films. *Nature Mater.* **2018**, *17*, 432. [CrossRef] [PubMed]
20. Zhang, Q.M.; Zhao, J.; Cross, L.E. Aging of the dielectric and piezoelectric properties of relaxor ferroelectric lead magnesium niobate–lead titanate in the electric field biased state. *J. Appl. Phys.* **1996**, *79*, 3181. [CrossRef]
21. Zhang, S.; Li, F.; Sherlock, N.P.; Luo, J.; Lee, H.J.; Xia, R.; Meyer, R.J., Jr.; Hackenberger, W.; Shrout, T.R. Recent developments on high Curie temperature PIN–PMN–PT ferroelectric crystals. *J. Cryst. Grow.* **2011**, *318*, 846. [CrossRef]
22. Qi, X.; Sun, E.; Lü, W.; Li, S.; Yang, B.; Zhang, R.; Cao, W. Dynamic characteristics of defect dipoles in Mn-doped $0.24Pb(In_{1/2}Nb_{1/2})O_3$–$0.47Pb(Mg_{1/3}Nb_{2/3})O_3$–$0.29PbTiO_3$ single crystal. *CrystEngComm* **2019**, *21*, 348. [CrossRef]
23. Genenko, Y.A.; Glaum, J.; Hoffmann, M.J.; Albe, K. Mechanisms of aging and fatigue in ferroelectrics. *Mater. Sci. Eng. B* **2015**, *192*, 52. [CrossRef]
24. Luo, N.; Zhang, S.; Li, Q.; Yan, Q.; Zhang, Y.; Ansell, T.; Luo, J.; Shrout, T.R. Crystallographic dependence of internal bias in domain engineered Mn-doped relaxor-$PbTiO_3$ single crystals. *J. Mater. Chem. C* **2016**, *4*, 4568–4576. [CrossRef]
25. Luo, L.; Dietze, M.; Solterbeck, C.-H.; Luo, H.-S.; Es-Souni, M. Tuning the functional properties of PMN-PT single crystals via doping and thermoelectrical treatments. *J. Appl. Phys.* **2013**, *114*, 224112. [CrossRef]
26. Kobor, D.; Guiffard, B.; Lebrun, L.; Hajjaji, A.; Guyomar, D. Oxygen vacancies effect on ionic conductivity and relaxation phenomenon in undoped and Mn doped PZN-4.5PT single crystals. *J. Phys. D Appl. Phys.* **2007**, *40*, 2920. [CrossRef]
27. Li, L.; Choudhury, S.; Liu, Z.K.; Chen, L.Q. Effect of external mechanical constraints on the phase diagram of epitaxial $PbZr_{1-x}Ti_xO_3$ thin films—Thermodynamic calculations and phase-field simulations. *Appl. Phys. Lett.* **2003**, *83*, 1608–1610. [CrossRef]
28. Olsen, R.B.; Bruno, D.A.; Briscoe, J.M. Pyroelectric conversion cycles. *J. Appl. Phys.* **1985**, *58*, 4709. [CrossRef]

29. Hunter, S.R.; Lavrik, N.V.; Bannuru, T.; Mostafa, S.; Rajic, S.; Datskos, P.G. Development of MEMS based pyroelectric thermal energy harvesters. In *Energy Harvesting and Storage: Materials, Devices, and Applications II*; Dhar, N.K., Wijewarnasuriya, P.S., Dutta, A.K., Eds.; SPIE: Bellingham, WA, USA, 2011; Volume 8035. [CrossRef]
30. Pandya, S.; Velarde, G.; Zhang, L.; Wilbur, J.D.; Smith, A.; Hanrahan, B.; Dames, C.; Martin, L.W. New approach to waste-heat energy harvesting: Pyroelectric energy conversion. *NPG Asia Mater.* **2019**, *11*, 26. [CrossRef]